

Image focus measure based on Chebyshev moments

P.T. Yap and P. Raveendran

Abstract: A new measure of image focus based on the discrete orthogonal Chebyshev moments is introduced. The low- and high-spatial-frequency components of an image can be represented as the low- and high-order Chebyshev moments, respectively. The focus measure is defined as the ratio of the norm of the high-order moments to that of low-order moments. It is shown that the focus measure is monotonic and unimodal with respect to image blurring. Additionally, it is invariant to contrast changes due to the differences in the intensities of illumination. The focus measure is tested for its discriminating power of images blurred to various degrees. Noise studies show that the focus measure is robust under Gaussian and salt-and-pepper noise. The performance of the proposed focus measure is compared with the existing focus measures.

1 Introduction

A clear and well-focused image is important in computer vision, astronomical imaging and microscopy [1–5]. For this reason, many focusing techniques have been investigated [6–8]. A focus measure is a quantity which measures the degree of blurring of an image; its value is a maximum when the image is best focused and decreases as blurring increases. It is particularly important in applications such as autofocus and depth recovery. Figure 1 shows the basic image formation geometry. All light rays radiated from point A of the object and intercepted by the lens are refracted to converge to a point B. For a thin lens, the relation between the object distance u , focal distance of the lens f and image distance v is given by

$$\frac{1}{u} + \frac{1}{v} = \frac{1}{f} \quad (1)$$

Each point on the object plane is projected onto a single point on the image plane, and thus a clear and focused image $f(x, y)$ is formed on the image plane. However, if the object is displaced by a distance d , the energy from the object through the lens is distributed over a circular patch on the image plane, resulting in a blurred image of the object. The blurred image $g(x, y)$ can be expressed as

$$g(x, y) = f(x, y) * h(x, y) \quad (2)$$

where $h(x, y)$ is the point-spread function (PSF) related to the blurring. Ideally, when $h(x, y) = \delta(x, y)$, we obtain the original image $g(x, y) = f(x, y)$. In practical situations, $h(x, y)$ has the characteristics of a lowpass filter. A focus measure reflects the amount of blurring introduced by $h(x, y)$. A typical focus measure should satisfy these requirements:

- independent of image content. The focus measure should not be based on particular structures of an image such as brightness and noise
- monotonic with respect to blur. The more blurred an image is, the smaller the value of the image focus measure should be
- the focus measure must be unimodal, that is, it must have one and only one maximum value. Since autofocus algorithms judge an image to be in focus by the maximum value of the function, multiple maxima lead to large focus error
- large variation in value with respect to the degree of blurring. Large usable range has a positive effect on the accuracy of the measure
- minimal computation complexity
- robust to noise.

Various focus measures were introduced in previous research literature [1, 3]. The common ones are M_1 : variance of image grey levels; M_2 : ℓ_1 -norm of image gradient; M_3 : ℓ_2 -norm of image gradient; M_4 : ℓ_1 -norm of second derivatives of image; and M_5 : energy of Laplacian of image. Most of them are measures of the high-spatial-frequency components of an image. This is due to the fact that the high-spatial-frequency components of an image are suppressed by blurring, regardless of the PSF.

To the best of our knowledge, no focus measure based on moments has been formulated. Moments and functions of moments have been widely used for pattern recognition [9, 10], pose estimation [11], signal modelling [12], image normalisation [13, 14] and image compression [15]. In this paper, a focus measure based on the Chebyshev moments is introduced. Mukundan *et al.* [16] introduced the notion of discrete orthogonal polynomials and showed that the set of Chebyshev moments can be used to capture the essential analytical properties of an image. The image information stored in each moment is independent and the information redundancy between the moments is minimal. Moreover, no numerical approximation is needed for evaluating the Chebyshev moments of discrete-space images. We use the set of Chebyshev moments to formulate a new noise-robust focus measure. Generally, the low-order Chebyshev moments capture the low-spatial-frequency components of an image, such as smooth surfaces which have a slow rate of variation in intensities. The high-order moments, on the

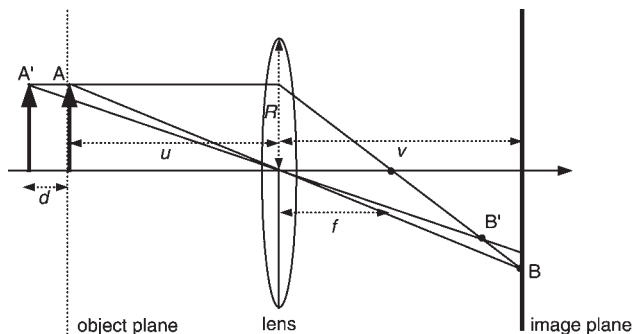


Fig. 1 Formation of focused and blurred images

other hand, capture those with high spatial frequency, such as edges and contours which have a high rate of variation in intensities. Based on this fact, the new focus measure is defined as the ratio of the norm of the high-order moments to the norm of the low-order moments. To demonstrate the discrimination power and robustness of the new focus measure, we compare the performance of the proposed focus measure with the existing focus measures.

2 Existing focus measures

Several focus measures were studied in [17, 2, 18]. Most of them are measures of the high-spatial-frequency components of an image. This is in accordance with the fact that blurring suppresses the high frequency information of an image regardless of the PSF. If the image is defined in the domain R . The simplest focus measure is the variance of image grey levels:

$$M_1 = \iint_R [g(x, y) - \mu]^2 dx dy \quad (3)$$

where μ is the mean of grey level values of $g(x, y)$. Several other focus measures are defined by the derivatives of the image. They are the:

ℓ_1 -norm of the image gradient:

$$M_2 = \iint_R \left| \frac{\partial g(x, y)}{\partial x} \right| + \left| \frac{\partial g(x, y)}{\partial y} \right| dx dy \quad (4)$$

ℓ_2 -norm of the image gradient:

$$M_3 = \iint_R \left[\frac{\partial g(x, y)}{\partial x} \right]^2 + \left[\frac{\partial g(x, y)}{\partial y} \right]^2 dx dy \quad (5)$$

ℓ_1 -norm of second derivatives of the image:

$$M_4 = \iint_R \left| \frac{\partial^2 g(x, y)}{\partial^2 x} \right| + \left| \frac{\partial^2 g(x, y)}{\partial^2 y} \right| dx dy \quad (6)$$

and energy of the Laplacian of the image:

$$M_5 = \iint_R \left[\frac{\partial^2 g(x, y)}{\partial^2 x} + \frac{\partial^2 g(x, y)}{\partial^2 y} \right]^2 dx dy \quad (7)$$

The monotonicity and unimodality of M_1 , M_3 and M_5 are proved by Subbarao *et al.* [1, 19]. It is shown that M_3 and M_5 are in fact measures of image energy after the Fourier spectrum $G(\omega, \nu)$ has been high-pass filtered by filters $\sqrt{(\omega^2 + \nu^2)}$ and $\omega^2 + \nu^2$, respectively. The definitions of the focus measures given above are summarised in Table 1. It should be noted that approximations are needed for actual implementation of the above-mentioned focus measures, since typical computer images have discrete-space domains. Some other focus measures can be found in [6].

Table 1: Definitions of existing focus measures

Description	Notation	Definition
Variance of image grey levels	M_1	$\iint (g(x, y) - \mu_i)^2 dx dy$
ℓ_1 -norm of image gradient	M_2	$\iint \left \frac{\partial g(x, y)}{\partial x} \right + \left \frac{\partial g(x, y)}{\partial y} \right dx dy$
ℓ_2 -norm of image gradient	M_3	$\iint \left[\frac{\partial g(x, y)}{\partial x} \right]^2 + \left[\frac{\partial g(x, y)}{\partial y} \right]^2 dx dy$
ℓ_1 -norm of second derivatives	M_4	$\iint \left \frac{\partial^2 g(x, y)}{\partial^2 x} \right + \left \frac{\partial^2 g(x, y)}{\partial^2 y} \right dx dy$
Energy of Laplacian of image	M_5	$\iint \left[\frac{\partial^2 g(x, y)}{\partial^2 x} + \frac{\partial^2 g(x, y)}{\partial^2 y} \right]^2 dx dy$

3 Chebyshev polynomials

The set of Chebyshev moments is based on the discrete Chebyshev polynomials [20–22, 16]. The n th-order N -point Chebyshev polynomial is defined as

$$t_n(x; N) = \sum_{k=0}^{N-1} a_{k,n} x^k = (1-N)_n {}_3F_2 \left(\begin{matrix} -n, -x, 1+n \\ 1, 1-N \end{matrix} \middle| 1 \right) \quad (8)$$

where $n, x = 0, 1, 2, \dots, N-1$, and

$${}_pF_q \left(\begin{matrix} a_1, \dots, a_p \\ b_1, \dots, b_q \end{matrix} \middle| z \right) = \sum_{k=0}^{\infty} \frac{(a_1)_k \dots (a_p)_k z^k}{(b_1)_k \dots (b_q)_k k!} \quad (9)$$

is the generalised hypergeometric function with the Pochhammer symbol defined as

$$(a)_k = \frac{\Gamma(a+k)}{\Gamma(a)} = a(a+1) \dots (a+k-1) \quad (10)$$

The set of N Chebyshev polynomials $\{t_n(x; N)\}$ forms a complete and finite set of discrete basis functions and satisfies the orthogonality condition

$$\sum_{x=0}^{N-1} t_m(x; N) t_n(x; N) = \rho(n; N) \delta_{mn} \quad (11)$$

where δ_{mn} is the Kronecker delta function and

$$\rho(n; N) = (2n)! \binom{N+n}{2n+1} \quad (12)$$

To speed up computation, the three-terms recurrence relation can be used:

$$t_n(x) = [(2n-1)(2x-N+1)t_{n-1}(x) - (n-1) \times (N^2 - (n-1)^2)t_{n-2}(x)]/n \quad (13)$$

where $n=2, 3, \dots, N-1$ and $t_0(x) = 1, t_1(x) = 1 - N + 2x$.

4 Chebyshev moments

The Chebyshev moment of order $(m+n)$ for an image with intensity function $f(x, y)$, $x \in \{0, 1, \dots, M-1\}$, $y \in \{0, 1, \dots, N-1\}$ is defined as

$$T_{mn} = \sum_{x=0}^{M-1} \sum_{y=0}^{N-1} \tilde{t}_m(x; M) \tilde{t}_n(y; N) f(x, y) \quad (14)$$

where $\tilde{t}_n(x; N)$ and $\tilde{t}_n(y; N)$ are the normalised Chebyshev polynomials defined by

$$\tilde{t}_m(x; M) = \frac{t_m(x; M)}{\sqrt{\rho(m; M)}}, \quad \tilde{t}_n(y; N) = \frac{t_n(y; N)}{\sqrt{\rho(n; N)}} \quad (15)$$

The set of Chebyshev moments satisfies the Parseval theorem, i.e.

$$\sum_{x=0}^{M-1} \sum_{y=0}^{N-1} [f(x, y)]^2 = \sum_{m=0}^{M-1} \sum_{n=0}^{N-1} [T_{mn}]^2 \quad (16)$$

4.1 Chebyshev moments as correlation measures

Correlation is a similarity measure between functions [23, 24]. The correlation of two discrete-space functions $r(x, y)$ and $s(x, y)$ is defined as

$$\rho_{rs} = \sum_{x=-\infty}^{\infty} \sum_{y=-\infty}^{\infty} r(x, y)[s(x, y)]^* \quad (17)$$

where $(\cdot)^*$ denotes the complex conjugate. If $r(x, y)$ and $s(x, y)$ are real, then (17) simply reduces to

$$\rho_{rs} = \sum_{x=-\infty}^{\infty} \sum_{y=-\infty}^{\infty} r(x, y)s(x, y) \quad (18)$$

If we let

$$\begin{aligned} s(x, y) &= f(x, y) \\ r(x, y) &= \tilde{t}_m(x; M)\tilde{t}_n(y; N) \end{aligned} \quad (19)$$

where $x = 0, 1, \dots, M-1$, $y = 0, 1, \dots, N-1$, then we have

$$\rho_{rs} = \sum_{x=0}^{M-1} \sum_{y=0}^{N-1} \tilde{t}_m(x; M)\tilde{t}_n(y; N)f(x, y) = T_{mn} \quad (20)$$

Hence, T_{mn} is in fact the correlation of the image and the moment kernel $\tilde{t}_m(x; M)\tilde{t}_n(y; N)$. In other words, Chebyshev moments measure the similarity between the image and the respective moment kernel. Generally, the spatial-frequency components measured by T_{mn} are dependent on the order $(m+n)$. The lower order moments measure the low-spatial-frequency components of an image, while the higher order moments measure the high-spatial-frequency components of an image. This shall be evident by observing the graphical plots of the moment kernels. For simplicity, we denote $\Phi_{mn} = \tilde{t}_m(x; M)\tilde{t}_n(y; N)$. Figure 2a shows the graphical plots of Φ_{22} . It can be seen that the moment kernel Φ_{22} is low in spatial frequency and hence T_{22} is a measure of the low-spatial-frequency component of an image. For $\Phi_{10,10}$, shown in Fig. 2b, the value of the moment kernel changes much more rapidly and hence $T_{10,10}$ extracts from the image the component with a higher spatial frequency.

4.2 Noise insensitivity of Chebyshev moments

The lower order Chebyshev moments are insensitive to noise. If the noise degraded image of $f(x, y)$ is denoted by $g(x, y)$, i.e.

$$g(x, y) = f(x, y) + n(x, y) \quad (21)$$

where $n(x, y)$ is the noise of the image, then the moments of $g(x, y)$ are

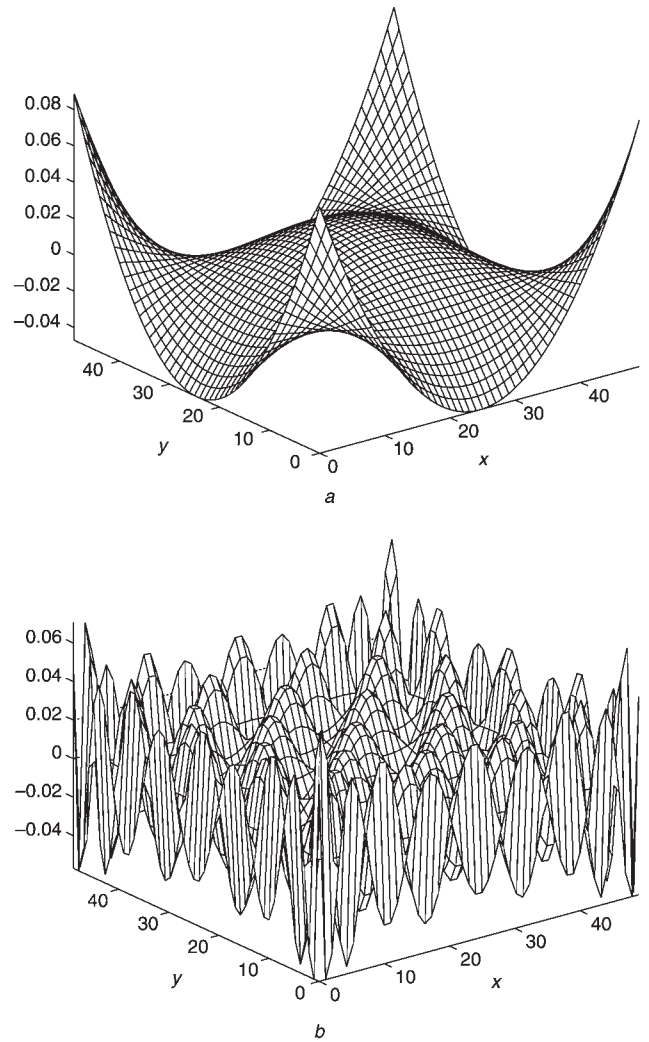


Fig. 2 Plots of kernel Φ_{mn}
 $M = N = 50$
a Φ_{22}
b $\Phi_{10,10}$

$$\begin{aligned} T_{mn}^{(g)} &= \sum_{x=0}^{M-1} \sum_{y=0}^{N-1} \tilde{t}_m(x; M)\tilde{t}_n(y; N)g(x, y) \\ &= \sum_{x=0}^{M-1} \sum_{y=0}^{N-1} \tilde{t}_m(x; M)\tilde{t}_n(y; N)f(x, y) \\ &\quad + \sum_{x=0}^{M-1} \sum_{y=0}^{N-1} \tilde{t}_m(x; M)\tilde{t}_n(y; N)n(x, y) \\ &\simeq T_{mn}^{(f)} \end{aligned} \quad (22)$$

since the correlations of low-spatial-frequency $\tilde{t}_m(x; M)\tilde{t}_n(y; N)$ and high-spatial-frequency $n(x, y)$ are typically small, i.e.

$$\sum_{x=0}^{M-1} \sum_{y=0}^{N-1} \tilde{t}_m(x; M)\tilde{t}_n(y; N)n(x, y) \simeq 0 \quad (23)$$

4.3 Implementation using matrix

In actual implementation, the Chebyshev moments are computed with the transformation matrix:

$$C_1 = \begin{pmatrix} \alpha_0 t_0(0) & \cdots & \alpha_0 t_0(M-1) \\ \vdots & \ddots & \vdots \\ \alpha_{M-1} t_{M-1}(0) & \cdots & \alpha_{M-1} t_{M-1}(M-1) \end{pmatrix} \quad (24)$$

$$C_2 = \begin{pmatrix} \alpha_0 t_0(0) & \cdots & \alpha_0 t_0(N-1) \\ \vdots & \ddots & \vdots \\ \alpha_{N-1} t_{N-1}(0) & \cdots & \alpha_{N-1} t_{N-1}(N-1) \end{pmatrix} \quad (25)$$

The set of Chebyshev moments of image $A = \{f(j, i)\}_{i,j=0}^{N-1}$ can be determined by

$$M = C_2 A C_1^T \quad (26)$$

where $(\cdot)^T$ denotes the transpose of the matrix and

$$M = \{T_{ij}\}_{i,j=0}^{M,N} \quad (27)$$

The matrix representation is very useful in software packages such as MATLAB. The transformation matrix C can be precomputed and stored to speed up the computation.

5 Chebyshev moments-based focus measure

The new focus measure is based on the Chebyshev moments. Given an $M \times N$ image $f(x, y)$, we normalise it by defining

$$\tilde{f}(x, y) = \frac{f(x, y)}{\sqrt{\sum_{x=0}^{M-1} \sum_{y=0}^{N-1} [f(x, y)]^2}} \quad (28)$$

so that

$$\sum_{x=0}^{M-1} \sum_{y=0}^{N-1} [\tilde{f}(x, y)]^2 = 1 \quad (29)$$

Note that this does not affect the spatial-frequency contents of the image. Based on $\tilde{f}(x, y)$ we have the corresponding set of Chebyshev moments $\mathbb{T}(\tilde{f}; M, N) = \{T_{mn}(\tilde{f})\}$, where $m = 0, 1, \dots, M-1$, $n = 0, 1, \dots, N-1$. We take the low-order moments to be moments of order less than P ($\leq M + N - 2$). Hence, if we denote the set of low- and high-order Chebyshev moments with $\mathbb{L}(\tilde{f}; P)$ and $\mathbb{H}(\tilde{f}; P)$, respectively, we have

$$\begin{aligned} \mathbb{L}(\tilde{f}; P) &= \{T_{kl} | k + l \leq P\}, \\ \mathbb{H}(\tilde{f}; P) &= \mathbb{T}(\tilde{f}) \setminus \mathbb{L}(\tilde{f}; P) \end{aligned} \quad (30)$$

where the operator \setminus denotes the set difference, i.e. $A \setminus B = \{x | x \in A \text{ and } x \notin B\}$.

We propose a Chebyshev moments-based focus measure:

$$M_T = \frac{\|\mathbb{H}(\tilde{f}; P)\|}{\|\mathbb{L}(\tilde{f}; P)\|} \quad (31)$$

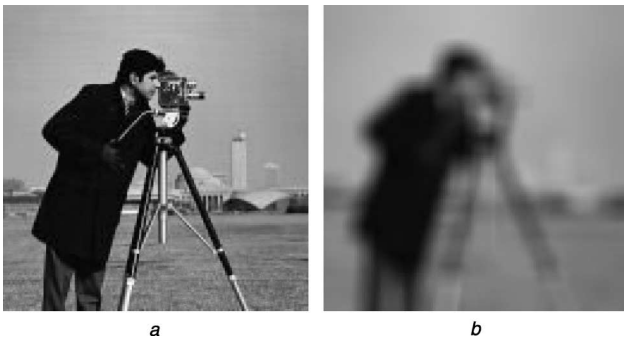


Fig. 3 'Camera man image'

a Original test image

b Blurred version of a with averaging mask $W \times W = 20 \times 20$

where $\|\cdot\|$ denotes the ℓ_2 -norm. The monotonicity of (31) can be understood intuitively. Since $\mathbb{L}(\tilde{f}; P)$ and $\mathbb{H}(\tilde{f}; P)$ identify the low-spatial-frequency (low-pass) and high-spatial-frequency (high-pass) components of the image, respectively, the proposed focus measure is in fact the

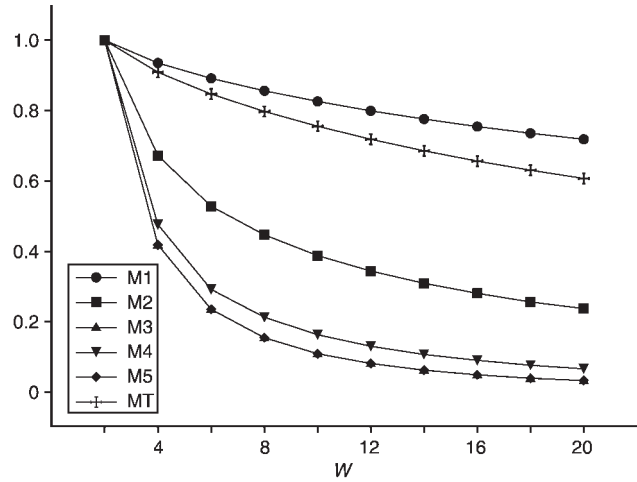


Fig. 4 Values of the various focus measures for images blurred with averaging masks of sizes $W \times W$, $W = 2, 4, \dots, 20$

Results are normalised for the purpose of comparison

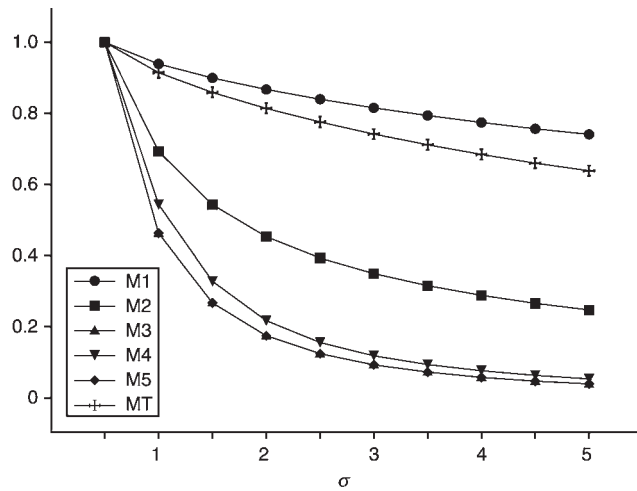


Fig. 5 Values of the various focus measures for images blurred with Gaussian function of standard deviation $\sigma = 0.5, 1.0, \dots, 5.0$

Results are normalised for the purpose of comparison

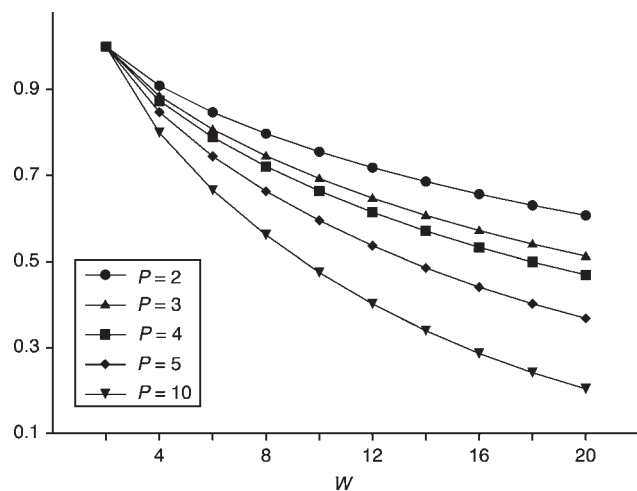


Fig. 6 Effect of parameter P on discriminating power

Table 2: Robustness of various focus measures under various degrees of noise

	σ/μ	
	Gaussian	Salt-and-pepper
M_1	0.0188	0.0589
M_2	0.2882	0.2691
M_3	0.2720	0.4841
M_4	0.3128	0.3238
M_5	0.2710	0.4765
M_T	0.0281	0.0908

measure of the ratio of the energies in high-pass band to the low-pass band. Generally, an image in focus has higher $\mathbb{H}(\tilde{f}; P)$ energy and lower $\mathbb{L}(\tilde{f}; P)$ when compared to a blurred image. For practical implementation, we can rewrite (31) as

$$M_T = \frac{\|\tilde{f}\| - \|\mathbb{L}(\tilde{f}; P)\|}{\|\mathbb{L}(\tilde{f}; P)\|} = \frac{1 - \|\mathbb{L}(\tilde{f}; P)\|}{\|\mathbb{L}(\tilde{f}; P)\|} \quad (32)$$

since, from (16), we have $\|\tilde{f}\| = \|\mathbb{L}(\tilde{f}; P)\| + \|\mathbb{H}(\tilde{f}; P)\|$.

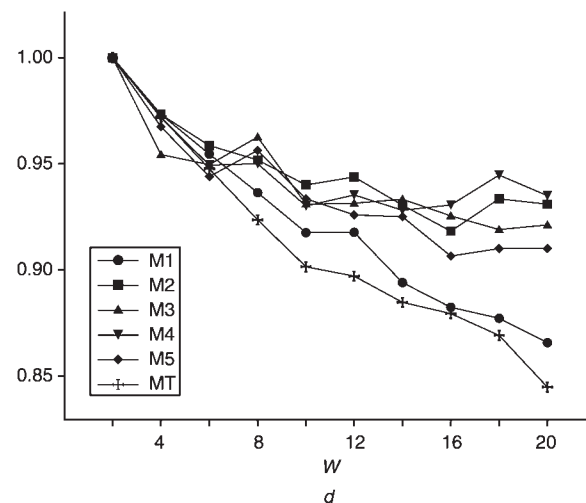
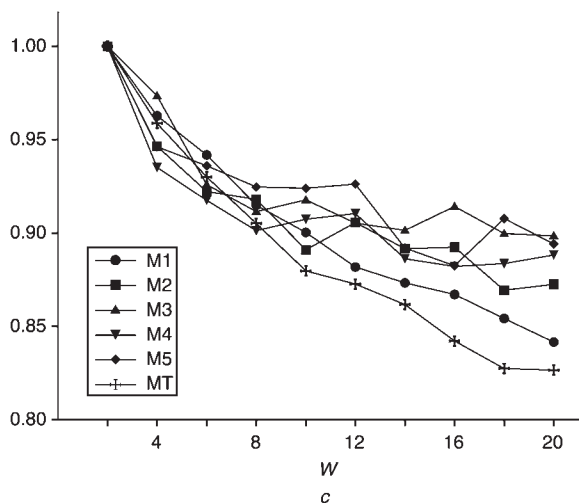
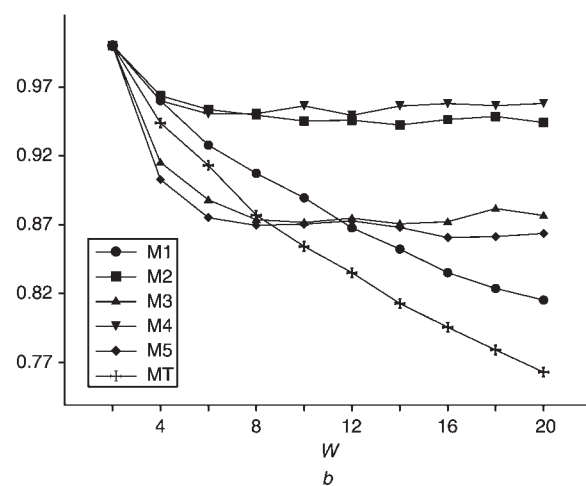
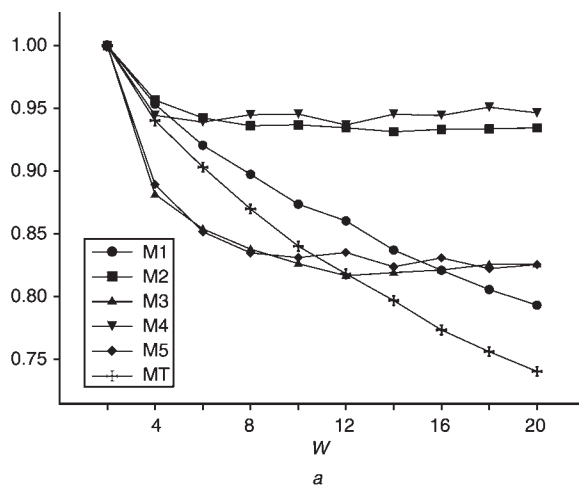


Fig. 8 Values of various focus measures for blurred images with Gaussian and salt-and-pepper noise

Results are normalised for the purpose of comparison. Average masks of sizes $W \times W$, $W = 2, 4, \dots, 20$ are used
 a With Gaussian noise of variance $V = 0.015$
 b With Gaussian noise of variance $V = 0.020$
 c With salt-and-pepper noise of density $D = 0.15$
 d With salt-and-pepper noise of density $D = 0.20$

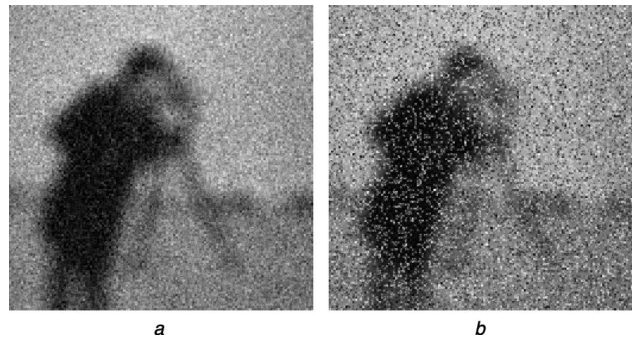


Fig. 7 Noise degraded images

a Blurred with averaging mask of size $W = 20$ and degraded with Gaussian noise of variance $\sigma^2 = 0.020$
 b Blurred with averaging mask of size $W = 20$ and degraded with salt-and-pepper noise of density $D = 0.20$

By using this (31), the computation of Chebyshev moments is reduced to those with order $\leq P$.

5.1 Effect of parameter P

If the parameter P is increased, the focus measure becomes more sensitive to the high frequency components of an image. This can be shown from the fact that from (32) we have

$$M_T^{(P)} = [\|\mathbb{L}(\tilde{f}; P)\|]^{-1} - 1 \quad (33)$$

and if P is increased by 1, then

$$M_T^{(P+1)} = \left[\|\mathbb{L}(\tilde{f}; P)\| + \sum_{s=0}^{P+1} \left(T_{P+1-s, s}^{(\tilde{f})} \right)^2 \right]^{-1} - 1 \quad (34)$$

This implies better discriminating power between various degrees of blurring, but it also means that the moments are more susceptible to the effect of noise. Hence, the value of P is to be set according to the context of application; compromise between the discriminating power and noise-robustness has to be made.

5.2 Monotonicity and unimodalness

Considering two images $f_1(x, y)$ and $f_2(x, y)$, and if $f_2(x, y)$ has a larger degree of blurring compared to $f_1(x, y)$, that is:

$$\begin{aligned} \|\mathbb{L}(\tilde{f}_2; P)\| &> \|\mathbb{L}(\tilde{f}_1; P)\| \\ \|\mathbb{H}(\tilde{f}_2; P)\| &< \|\mathbb{H}(\tilde{f}_1; P)\| \end{aligned} \quad (35)$$

we have

$$M_T^{(f_2)} = \frac{\|\mathbb{H}(\tilde{f}_2; P)\|}{\|\mathbb{L}(\tilde{f}_2; P)\|} < M_T^{(f_1)} = \frac{\|\mathbb{H}(\tilde{f}_1; P)\|}{\|\mathbb{L}(\tilde{f}_1; P)\|} \quad (36)$$

Hence, we conclude that the proposed focus measure M_T is monotonic. The unimodality of M_T is inherently proved by its monotonicity.

5.3 Noise robustness

As shown in Section 4.2, the lower order Chebyshev moments are insensitive to noise. Hence, for a small P , it can be easily shown that, for a noise-degraded image $g(x, y)$ of $f(x, y)$, we have

$$M_T^{(\tilde{g})} = \frac{1 - \|\mathbb{L}(\tilde{g}; P)\|}{\|\mathbb{L}(\tilde{g}; P)\|} \simeq \frac{1 - \|\mathbb{L}(\tilde{f}; P)\|}{\|\mathbb{L}(\tilde{f}; P)\|} = M_T^{(\tilde{f})} \quad (37)$$

since $\|\mathbb{L}(\tilde{g}; P)\| \simeq \|\mathbb{L}(\tilde{f}; P)\|$.

5.4 Contrast invariance

If the contrast of the original image $f(x, y)$ is modified by a factor k , i.e. the modified image $g(x, y)$ is $g(x, y) = kf(x, y)$, then the focus measure is

$$M_T^{(\tilde{g})} = \frac{\|\mathbb{H}(\tilde{g}; P)\|}{\|\mathbb{L}(\tilde{g}; P)\|} = \frac{\|\mathbb{H}(\tilde{f}; P)\|}{\|\mathbb{L}(\tilde{f}; P)\|} \quad (38)$$

since

$$\begin{aligned} \tilde{g}(x, y) &= \frac{g(x, y)}{\sqrt{\sum_{x=0}^{M-1} \sum_{y=0}^{N-1} [g(x, y)]^2}} \\ &= \frac{kf(x, y)}{\sqrt{\sum_{x=0}^{M-1} \sum_{y=0}^{N-1} [kf(x, y)]^2}} = \tilde{f}(x, y) \end{aligned} \quad (39)$$



Fig. 9 Whole set of test images

Hence, the proposed focus measure is invariant to contrast changes of an image. This is especially important for conditions where the intensity of the illumination changes.

6 Experimental studies

In this Section, we provide experimental results of the performance of the proposed focus measure. Note that M_1 , M_2 , M_3 , M_4 and M_5 are as denoted in Table 1. M_T denotes the proposed focus measure, which is based on the set of Chebyshev moments. Unless otherwise mentioned, we take $P = 2$.

6.1 Noise-free images

To test the effectiveness of the proposed focus measure, we compare its performance with the existing focus measures. The ‘Camera man’ image (256×256), shown in Fig. 3a, is blurred by using averaging masks of different sizes $W \times W = 2 \times 2, 4 \times 4, \dots, 20 \times 20$. A larger size W of the mask signifies a greater degree of blurring. The performance of the proposed focus measure is then tested with the existing focus measures, and the results are shown

in Fig. 4. It can be seen that all the focus measures are monotonic, that is, all the values of the focus measures decrease with the degree of blurring. Figure 5 shows the results of the proposed focus measure when the image is blurred with the Gaussian function [25] of standard deviation $\sigma = 0.5, 1.0, \dots, 5.0$. The results are similar to those of Fig. 4.

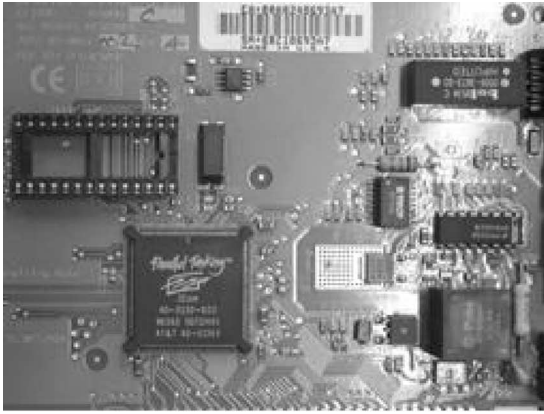
The sensitivity of the proposed focus measure to the high-spatial-frequency components is determined by the parameter P . Figure 6 shows the effect of P on the discriminating power; the higher the value of P , the higher the discriminating power of the focus measure with regard to the degree of blurring.

6.2 Images degraded with noise

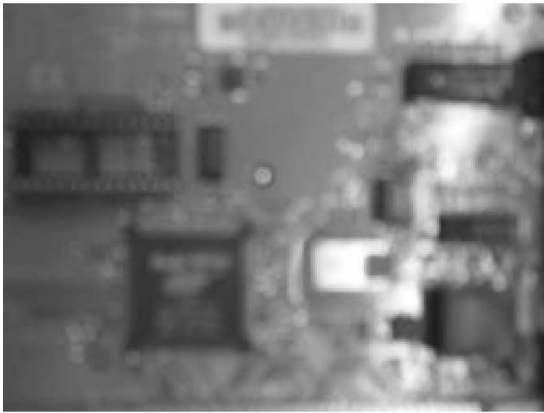
Visual equipment is often not without flaw and may introduce noise to the captured image. This increases the high-spatial-frequency components of the image and causes the focus measure to erroneously take a noisy blurred image as a focused image. To simulate and test the performance of the proposed focus measure under such noisy conditions, Gaussian white noise of variances, $V = 0.005, 0.020$, and

Table 3: Normalised values of M_T for blurred images

a Noise-free										
Image	2×2	4×4	6×6	8×8	10×10	12×12	14×14	16×16	18×18	20×20
1	1.0000	0.9104	0.8486	0.7991	0.7569	0.7199	0.6871	0.6579	0.6320	0.6085
2	1.0000	0.9391	0.8767	0.8161	0.7591	0.7058	0.6561	0.6103	0.5678	0.5285
3	1.0000	0.8529	0.7827	0.7331	0.6939	0.6602	0.6301	0.6022	0.5755	0.5501
4	1.0000	0.8902	0.8138	0.7522	0.6990	0.6526	0.6120	0.5759	0.5438	0.5150
5	1.0000	0.8974	0.8203	0.7576	0.7066	0.6644	0.6282	0.5964	0.5676	0.5411
6	1.0000	0.9343	0.8708	0.8110	0.7558	0.7047	0.6577	0.6142	0.5743	0.5377
7	1.0000	0.9196	0.8546	0.7953	0.7413	0.6921	0.6469	0.6056	0.5681	0.5339
8	1.0000	0.9507	0.9014	0.8532	0.8069	0.7623	0.7202	0.6809	0.6445	0.6111
9	1.0000	0.3808	0.2561	0.2034	0.1612	0.1399	0.1229	0.1076	0.0999	0.0899
b Images are degraded with Gaussian noise of variance 0.05										
Image	2×2	4×4	6×6	8×8	10×10	12×12	14×14	16×16	18×18	20×20
1	1.0000	0.9224	0.8710	0.8292	0.7877	0.7543	0.7305	0.7062	0.6798	0.6602
2	1.0000	0.9541	0.9062	0.8649	0.8217	0.7793	0.7445	0.7085	0.6804	0.6477
3	1.0000	0.8906	0.8326	0.7958	0.7630	0.7363	0.7180	0.6918	0.6784	0.6589
4	1.0000	0.9135	0.8430	0.7898	0.7521	0.7074	0.6714	0.6439	0.6185	0.5914
5	1.0000	0.9212	0.8547	0.8109	0.7714	0.7378	0.7102	0.6811	0.6627	0.6412
6	1.0000	0.9493	0.8925	0.8384	0.7938	0.7498	0.7057	0.6705	0.6368	0.6041
7	1.0000	0.9339	0.8755	0.8225	0.7797	0.7371	0.6971	0.6608	0.6279	0.5935
8	1.0000	0.9682	0.9195	0.8845	0.8521	0.8163	0.7839	0.7484	0.7250	0.6992
9	1.0000	0.5356	0.4420	0.4016	0.3687	0.3528	0.3340	0.3232	0.3177	0.3147
c Images are degraded with salt-and-pepper noise of density 0.15										
Image	2×2	4×4	6×6	8×8	10×10	12×12	14×14	16×16	18×18	20×20
1	1.0000	0.9554	0.9256	0.9010	0.8754	0.8737	0.8477	0.8340	0.8181	0.8155
2	1.0000	0.9958	0.9622	0.9466	0.9411	0.9169	0.9072	0.9042	0.8960	0.8859
3	1.0000	0.9711	0.9603	0.9367	0.9168	0.9235	0.9076	0.9075	0.8931	0.8914
4	1.0000	0.9584	0.9340	0.9169	0.8872	0.8827	0.8689	0.8457	0.8471	0.8340
5	1.0000	0.9733	0.9451	0.9350	0.9197	0.9128	0.8981	0.8909	0.8843	0.8712
6	1.0000	0.9608	0.9332	0.9135	0.8817	0.8670	0.8308	0.8183	0.7932	0.7780
7	1.0000	0.9700	0.9404	0.9134	0.8962	0.8806	0.8496	0.8333	0.8177	0.8060
8	1.0000	0.9844	0.9834	0.9712	0.9555	0.9492	0.9330	0.9176	0.8924	0.8856
9	1.0000	0.8498	0.8014	0.7864	0.7906	0.7675	0.7678	0.7657	0.7659	0.7649



a



b



c

Fig. 10 Images from camera

$M \times N = 256 \times 192$

a Focused image, $M_T = 1.000$

b Medium out-of-focus, $M_T = 0.9011$

c Heavy out-of-focus, $M_T = 0.7716$

Proportional values are used: 1 stands for best focused image

salt-and-pepper noise of densities, $D = 0.15, 0.20$, are added to the blurred images (such as Fig. 3b). A sample image for each type of noise is shown in Fig. 7.

Figures 8a and 8b show the values of the focus measures for M_1, M_2, M_3, M_4, M_5 and M_T for the case of Gaussian noise. Figures 8c and 8d show the values of the focus measures for the case of salt-and-pepper noise. An ideal focus measure should decrease with the degree of blurring even under noisy conditions. The larger the difference between consecutive values, the better the discrimination power of the measure. It can be observed that, compared to other focus measures, the proposed focus measure has a higher discrimination power. As the degree of blurring increases, the value of M_T decreases regardless of the noise. Focus measures M_2, M_3, M_4, M_5 tend to lose the discrimination power and monotonicity as the degree of blurring increases. When comparing M_T with M_1 , the steeper slope of the former implies that consecutive values of M_T differ more when compared to M_1 . Hence it can be concluded that M_T has the highest discrimination power among the studied focus measures under noisy conditions.

Table 2 shows the spread σ/μ for the various focus measures under various noise conditions.

The values obtained are based on these conditions: Gaussian noise of variance 0.001, 0.002, ..., 0.005 and salt-and-pepper of density 0.01, 0.02, ..., 0.05. It can be seen that the proposed focus measure is more robust to noise compared to the other focus measures, although it is marginally less robust when compared to M_1 .

The proposed focus measure is tested with other images; the whole set of test images is shown in Fig. 9. Table 3 shows the values of M_T for the noise free condition and when the images are degraded by Gaussian or salt-and-pepper noise. It can be observed that for all cases, except for the last case (c) in the Table, the proposed focus measure is monotonic and unimodal.

6.3 Real images

The proposed focus measure is also tested with real images taken as shown in Fig. 10. Taken with a Canon PowerShot G2 digital camera at different focal lengths, the images are rescaled to size $M \times N = 256 \times 192$ and all the images are converted to grey level images by eliminating the hue and saturation information while retaining the luminance. It can be observed that the value of M_T decreases with the increase in the degree of blurring.

6.4 Contrast invariance

Owing to the fact that the intensity of illumination tends to vary, a focus measure which is contrast invariant is desirable. Table 4 shows the spread σ/μ of the focus measures for different intensities of illumination. The intensity changes are simulated by considering the modified image:

Table 4: Contrast invariance of proposed focus measures

k	0.1	0.2	0.3	0.4	0.5	0.6	0.7	0.8	0.9	1.0	σ/μ
$M_1 (\times 10^8)$	0.0257	0.1018	0.2290	0.4072	0.6367	0.9175	1.2487	1.6307	2.0618	2.5470	0.8875
$M_2 (\times 10^5)$	0.8279	1.6357	2.4613	3.2721	4.0969	4.9202	5.7389	6.5566	7.3723	8.1922	0.5501
$M_3 (\times 10^7)$	0.0288	0.1133	0.2544	0.4515	0.7054	1.0160	1.3827	1.8052	2.2848	2.8200	0.8871
$M_4 (\times 10^5)$	0.7059	1.3770	2.0569	2.7267	3.4049	4.0862	4.7641	5.4385	6.1128	6.7875	0.5466
$M_5 (\times 10^7)$	0.0288	0.1133	0.2544	0.4515	0.7054	1.0160	1.3827	1.8052	2.2848	2.8200	0.8871
M_T	0.1848	0.1844	0.1840	0.1845	0.1832	0.1848	0.1845	0.1847	0.1843	0.1846	0.0026

Table 5: Average computation time of various focus measures

Focus measure	Computation time, ms
M_1	6.25
M_2	67.85
M_3	64.10
M_4	175.05
M_5	177.30
M_T	8.50

$$g(x, y) = \text{round}[kf(x, y)] \quad (40)$$

The values are rounded, as digital images have quantised intensity values. From the Table, it can be observed that the proposed focus measure M_T is invariant to contrast changes due to the change of intensity of illumination.

6.5 Computation speed

Experimental results also show that M_T has a higher computation speed when compared to other focus measures; except M_1 , which is marginally faster. This is an advantage for real-time implementations. The average computation times of all the focus measures are shown in Table 5. The computations are done on a PC with a 2.27 GHz Pentium 4 processor and 256 MB RAM, using the ‘camera man’ image.

7 Conclusion

In this paper, a new measure of image focus based on Chebyshev moments is proposed. The low- and high-order Chebyshev moments capture the smooth and fine structures of an image, respectively. We define the new focus measure as the ratio of the norm of the low order moments to that of the high order moments. The new focus measure has a high discrimination power despite the noises introduced in the image. Moreover, no numerical approximation is involved in the computation the focus measure for discrete-space images. Comparisons are done with existing focus measures, and experimental results show that the Chebyshev moments-based focus measures perform significantly better in terms of discrimination power, noise robustness, contrast invariance and computation time.

8 Acknowledgments

The authors would like to thank the anonymous reviewers for their time in reviewing and providing valuable

comments on this paper. They would also like to thank FreeFoto.com (www.freefoto.com) for providing the ‘Wall’ image used in Fig. 9.

9 References

- Subbarao, M., Choi, T., and Nikzad, A.: ‘Focusing techniques’, *Proc. SPIE-Int. Soc. Opt. Eng.*, 1992, **1823**, pp. 163–174
- Subbarao, M., and Tyan, J.: ‘Selecting the optimal focus measure for autofocusing and depth-from-focus’, *IEEE Trans. Pattern Anal. Mach. Intell.*, 1998, **20**, (8), pp. 864–870
- Kautsky, J., Flusser, J., and Zitová, S.v.B.: ‘A new wavelet-based measure of image focus’, *Pattern Recognit. Lett.*, 2002, **23**, pp. 1785–1794
- Lee, J., Kim, K., Nam, B., Lee, J., Kwon, Y., and Kim, H.: ‘Implementation of a passive automatic focusing algorithm for digital still camera’, *IEEE Trans. Consum. Electron.*, 1995, **41**, (3), pp. 449–454
- Dias, J., Almeida, A., and Araújo, H.: ‘Depth recovery using active focus robotics’. *Proc. IROS ’91*, 1991, vol. 1, pp. 249–255
- Krotkov, E.: ‘Focusing’, *Int. J. Comput. Vis.*, 1987, **1**, pp. 223–237
- Lighthart, G., and Groen, F.: ‘A comparison of different autofocus algorithms’. *Proc. Int. Conf. on Pattern Recognition*, 1982, pp. 597–600
- Schlag, J., Sanderson, A., Neuman, C., and Wimberly, F.: ‘Implementation of automatic focus algorithms for a computer vision system with camera control’. CMU-RI-TR-83-14, Robotics Institute, Carnegie-Mellon University
- Hu, M.: ‘Visual pattern recognition by moment invariants’, *IRE Trans. Inf. Theory*, 1962, **IT-8**, pp. 179–187
- Teague, M.: ‘Image analysis via the general theory of moments’, *J. Opt. Soc. Am.*, 1962, **70**, pp. 920–930
- Mukundan, R., and Ramakrishnan, K.: ‘Moment functions in image analysis’ (World Scientific Publishing, Singapore, 1998)
- Iskander, D., Collins, M., and Davis, B.: ‘Optimal modeling of corneal surfaces with zernike polynomials’, *IEEE Trans. Biomed. Eng.*, 2001, **48**, (1), pp. 87–95
- Abu-Mostafa, Y., and Psaltis, D.: ‘Image normalization by complex moments’, *IEEE Trans. Pattern Anal. Mach. Intell.*, 1985, **7**, pp. 46–55
- Rothe, I., Süsse, H., and Voss, K.: ‘The method of normalization to determine invariants’, *IEEE Trans. Pattern Anal. Mach. Intell.*, 1996, **18**, (4), pp. 366–376
- Yap, P., and Raveendran, P.: ‘Image compression using discrete tchebichef transform with zonal coding’. *Proc. AIAI 2003*, 2003
- Mukundan, R., Ong, S., and Lee, P.: ‘Image analysis by Chebyshev moments’, *IEEE Trans. Image Process.*, 2001, **10**, (9), pp. 1357–1364
- Subbarao, M., and Choi, T.: ‘Accurate recovery of three-dimensional shape from image focus’, *IEEE Trans. Pattern Anal. Mach. Intell.*, 1995, **17**, (3), pp. 266–274
- Nayar, S., and Nakagawa, Y.: ‘Shape from focus’, *IEEE Trans. Pattern Anal. Mach. Intell.*, 1994, **16**, (8), pp. 824–831
- Subbarao, M., Choi, T.S., and Nikzad, A.: ‘Focusing techniques’, *J. Opt. Eng.*, 1993, pp. 2824–2836
- Koekoek, R., and Swarttouw, R.: ‘The askey-scheme of hypergeometric orthogonal polynomials and its q-analogue’. Technische Universiteit Delft, Faculty of Technical Mathematics and Informatics Report 98-17, 1998, pp. 46–47
- Erdelyi, A., Magnus, W., Oberhettinger, F., and Tricomi, F.G.: ‘Higher transcendental functions’ (McGraw-Hill, New York, USA, 1953)
- Szegő, G.: ‘Orthogonal polynomials’ (American Mathematical Society, New York, USA, 1939)
- Hayes, M.: ‘Statistical digital signal processing and modeling’ (John Wiley & Sons, 1995)
- Manolakis, D., Ingle, V., and Kogon, S.: ‘Statistical and adaptive signal processing’ (McGraw Hill, Singapore, 2000)
- Petrou, P.B.M.: ‘Image processing: the fundamentals’ (John Wiley & Sons, 1999)